Structure and dynamics of water confined in single-wall carbon nanotubes

2006 J. Phys.: Condens. Matter 18 S2321

(http://iopscience.iop.org/0953-8984/18/36/S07)

INSTITUTE OF PHYSICS PUBLISHING JOURNAL OF PHYSICS: CONDENSED MATTER

J. Phys.: Condens. Matter **18** (2006) S2321–S2334 doi:10.1088/0953-8984/18/36/S07

Structure and dynamics of water confined in single-wall carbon nanotubes

N R de Souza[1], A I Kolesnikov[1], C J Burnham[2] and C-K Loong[1,3]

[1] Intense Pulsed Neutron Source Division, Argonne National Laboratory, Argonne, IL 60439, USA
[2] Physics Department, University of Houston, Houston, TX 77204, USA

E-mail: ckloong@anl.gov

Received 9 March 2006
Published 24 August 2006
Online at stacks.iop.org/JPhysCM/18/S2321

Abstract

The structure and dynamics of water confined in open-ended single-wall carbon nanotubes (SWNTs), here referred to as nanotube-water, were investigated by a combined neutron-scattering and molecular-dynamics-simulation study. A 'shell + chain' configuration of nanotube-water that is consistent with both experimental observations and simulation results was identified at low temperatures. The shell consists of a square-ice sheet rolled into a hollow cylinder inside an SWNT in a tube-in-tube configuration. The chain along the centreline of the shell comprises a single file of water molecules. Large fluctuations via hydrogen-bond breaking/formation, including those associated with molecules between the shell and the chain, prevail even at very low temperatures and the resulting overall hydrogen-bond network of nanotube-water is weakened significantly. Hydrogen bonds associated with the chain are especially pliable. The fluctuations increase drastically with temperature, leading to the disappearance of the shell–chain structure at ∼210 K and the realization of confined supercooled water. A comparison of the hydrogen-bond energetics and relaxation processes of nanotube-water with those of confined supercooled water in porous silica MCM-41-S is discussed.

(Some figures in this article are in colour only in the electronic version)

1. Introduction

Liquids confined in a nanoscale environment exhibit unique properties that are of interest to a large research community, both fundamentally and technologically, as illustrated by many papers in this special issue of the journal. Water under confinement, with its paramount importance and complex functions in nature, from cosmology to mineralogy to biology, commands enduring investigations. The underlying control factors are the topology of the encapsulating medium, structural and dynamic fluctuations associated with hydrogen bonds,

[3] Author to whom any correspondence should be addressed.

and the nature of atomic interactions at the interface. Characterization of these key elements has been challenging because the technique employed has to resolve distances and events characteristic of intra- and intermolecular vibrations as well as atomic diffusion over the landscape of the confined geometry. The combination of neutron scattering and computer simulation offers advantageous elemental sensitivity and spatial–temporal resolution that are essential to the study.

Water encapsulated in mesoporous silica such as MCM-41-S that features cylindrical pores of about 14 Å in diameter has attracted much attention. Nanoscale confinement enables the survival of supercooled water, i.e., bypassing the homogeneous nucleation of ice, to a region at extended temperatures and pressures—the so-called 'no man's land' where the anomalous behaviour of water becomes most pronounced [1, 2] but virtually no experimental data ever existed previously. Thus the recent finding of evidence of a fragile-to-strong liquid–liquid transition and possibly a second critical point in supercooled water realized by confinement in MCM-41-S is remarkable [3, 4]. In oxide-based confining media such as silica or zeolites, the hydrophilic surfaces of the pores give rise to the dichotomy of lower density–slower dynamics of an interfacial water layer and higher density–faster dynamics of bulk water away from the substrate [5]. The substantial decrease in density of the interfacial water is the result of hydrophilic interaction that strongly distorts the hydrogen-bond network configuration of bulk water. In the case of hydrophobic liquid–water interfaces such as CCl_4/H_2O and hexane/H_2O, the hydrogen bonds between water molecules are sufficiently weakened to allow the manifestation of the secondary dipole–multipole interaction between a water molecule and a molecule in the substrate [6].

Water encapsulated in carbon nanotubes represents an interesting scenario contrasting to water in oxide-based porous media. First, unlike the strong interaction between water molecules and the oxide surfaces coated with chemisorbed hydroxyl groups in silica, the nanotube walls are hydrophobic and interactions between the water molecules and the carbon atoms are weak [7]. Second, the quasi-one-dimensional geometry of the nanotube environment differs from the internal pores that form an inter-connected framework in porous silica and zeolites. Finally, the highly anisotropic force fields with respect to the directions parallel and perpendicular to the nanotube axis are expected to engender a hydrogen-bond network configuration that is drastically different from that of water confined in silica pores, and consequently supercooled water in nanotubes may exhibit very dissimilar thermodynamic behaviour. Furthermore, water in carbon nanotubes provides a simplified model for studying water/proton transport across biological membranes. The crucial factors there are modified hydrogen bonding of water in confined channels of transmembrane proteins and dynamic fluctuations involving water molecules in the nominally hydrophobic environment [8–10].

The structure and dynamics of confined water in carbon nanotubes have not been studied as extensively as in the case of water in porous silica but initial investigations have revealed some intriguing phenomena. Here, we present the results from a combined neutron-scattering and molecular-dynamics (MD) simulation study. Section 2 describes the materials, neutron experiments, and the MD method. Section 3 presents the experimental results, and this is followed by a discussion of the observed data in comparison with the MD simulations in section 4. Some concluding remarks are given in section 5.

2. Materials, experimental details, and simulations

2.1. Single-wall open-ended carbon nanotubes (SWNT)

Powder samples of single-wall open-ended carbon nanotubes were prepared by the MER Corporation (Tucson, Arizona) using a conventional method of direct-current arc vaporization

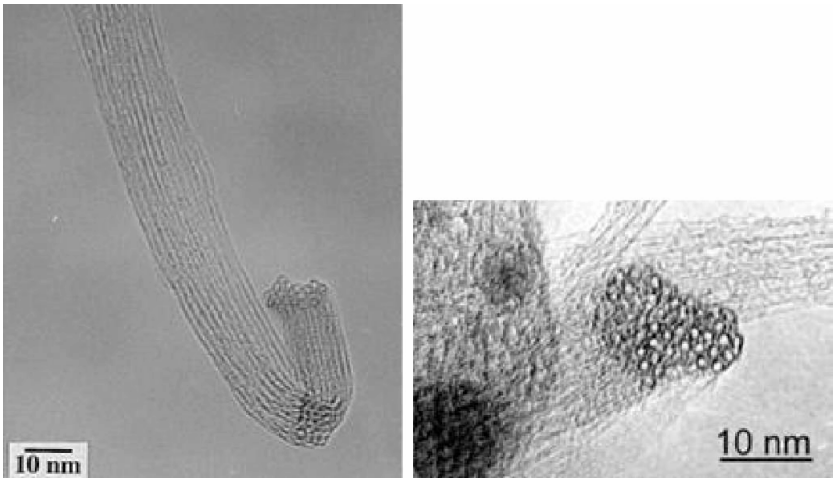

Figure 1. TEM images of open-ended SWNTs. A single bundle of SWNTs (left) and a close-up of the nanotube terminals (right). The hexagonal symmetry of the nanotube terminals of a bundle is visible in both images.

of graphite–metal composite anodes, followed by purification processes for the removal of metal catalyst residuals and non-tube carbon components [11]. The nanotube ends were opened by exposing the purified materials to air at 420 °C for ∼30 min. The structure of the SWNTs was characterized by electron microscopy, Raman scattering and neutron diffraction. Figure 1 shows transmission electron microscopy (TEM) images which confirm the open-endedness of individual SWNTs and the formation of a typical bundle with a cross section of nanotube terminals in hexagonal symmetry. The lengths of the bundles vary but are of the order of 10 μm. Neutron diffraction revealed the (01) reflection of the 2D hexagonal lattice of the bundle, as seen in figure 2(a) (dry SWNT). The estimated mean diameter of the SWNTs is 14 ± 1 Å. In common with most purified carbon nanotube materials, our SWNT samples contain typical impurities of Co and Ni nanoparticles up to about 3 wt% in total and the nanotubes exhibit local defects (holes, cross-links, etc). For the gram-quantity samples in use here it is irrelevant to classify the overall structure of the SWNTs by a unique (n, m) index or a specific helicity. In any event, the presence of such residual impurities, local defects and varying microstructure does not affect the interpretation of the neutron data regarding the encapsulated water, because the low impurity concentration and much larger length scale of the microstructure/defects than the water molecules only lead to a negligible and featureless background in the neutron intensity.

The introduction of water in SWNTs was administered following an identical protocol for all samples: a mixture of excess de-ionized H_2O or D_2O (99.9% pure, MSD Isotopes, Montreal, Canada) water and the nanotube material was equilibrated for 2 h in an enclosed volume at 110 °C; external free water adsorbed on the surfaces of the bundles or in the voids external to the nanotubes was then evaporated at 45 °C until reaching the targeted water mass fraction, signifying the remaining of only encapsulated water inside the SWNTs, to which we refer as 'nanotube-water'. The verification of the nanotube-water configuration by neutron diffraction is described in section 3.1.

2.2. Neutron scattering experiments

The neutron measurements were performed on the Small-Angle Neutron Diffractometer (SAND), the High-Resolution Medium-Energy Chopper Spectrometer (HRMECS) and the

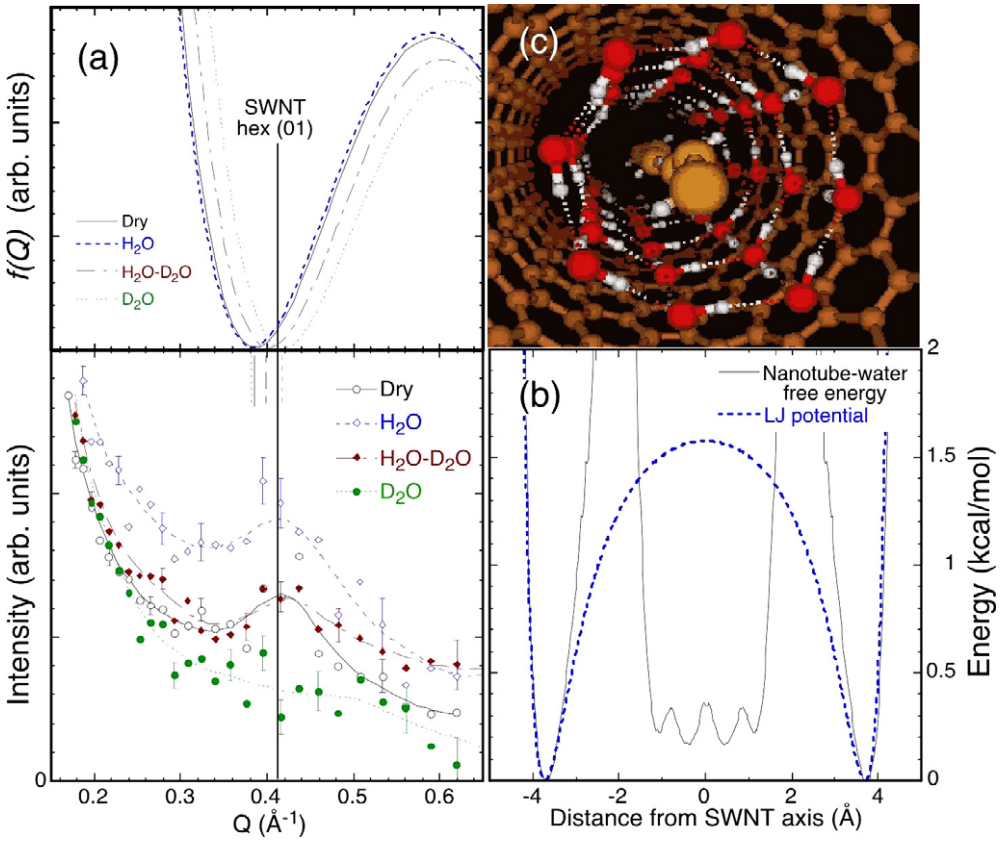

Figure 2. (a) The observed SAND intensities from the dry, H_2O-, D_2O-, and 50% H_2O–50% D_2O-filled SWNT samples at 278 K (bottom). The lines are guides to the eye, and for clarity errors are shown only at selected data points. The vertical line indicates the position of the (01) Bragg reflection from the nanotube bundles where a peak is expected provided that it does not coincide with the zero of the form factor, $f(Q)$ (top). The shift of the $f(Q)$ zeros (short tick marks) for the samples, calculated based on water *inside* the SWNTs, explains the change of intensity (see text). (b) The free energy of nanotube-water at 100 K and LJ potential for carbon–water interaction for MD simulations. (c) The static structure of nanotube-water at 100 K showing water molecules in the shell–chain configuration inside an SWNT.

QuasiElastic Neutron Spectrometer (QENS), all at the Intense Pulsed Neutron Source (IPNS) of Argonne National Laboratory. The SAND measurements, typically using a ∼50 mg sample, provide accurate diffraction data over a wide Q-range, especially around the (01) reflection peak of the SWNT bundles with and without water. This allows the comparison with calculated neutron intensities for different scenarios of encapsulated or externally adsorbed water.

The HRMECS and QENS enable inelastic-scattering measurements of the nanotube-water over a wide (Q, E) range, where Q and E are the neutron wavevector and energy transfer, respectively. The HRMECS, being a direct-geometry time-of-flight spectrometer operating at fixed (selected) incident neutron energy E_0, yields an energy resolution $\Delta E/E_0$ varying from about 4% at the elastic region to about 2% near the end of the neutron energy-loss spectrum. Therefore, by choosing different incident energies, e.g., 50, 140, and 600 meV, the entire inter- and intramolecular vibrational spectrum of nanotube-water can be measured with good resolution. Moreover, owing to the much larger incoherent neutron scattering cross section of

H atoms compared to those of O and C, the obtained HRMECS inelastic spectra summed over the detector angles effectively yield a spectrum almost entirely due to the dynamics of hydrogen motion. It contains mainly the neutron-weighted vibrational density-of-states (DOS) of the fundamental modes and, to a lesser degree, the combined excitations of fundamental modes and higher-order overtones [12]. The observed spectrum, notwithstanding the combination-mode contributions, can be compared with the corresponding DOS of fundamental modes from MD simulations in a straightforward manner. The data obtained at small scattering angles (small Q-values) with high incident energies were crucial to the measurements of the DOS due to the extraordinarily large mean-square displacement of hydrogen $\langle u_{\mathrm{H}}^2 \rangle$ which severely damps the intensity with increasing Q, according to $\sim \exp(-\langle u_{\mathrm{H}}^2 \rangle Q^2)$.

The QENS is an inverse-geometry time-of-flight crystal-analyser spectrometer designed to achieve the best energy resolution ($\Delta E = 80\ \mu$eV) near the elastic region. The elastic intensity, $I(Q, E = 0)$, of incoherent scattering from hydrogen atoms follows the expression

$$\ln[I(Q, E = 0)] = I_0 - \langle u_{\mathrm{H}}^2 \rangle Q^2, \tag{1}$$

where I_0 is a constant. The good energy resolution of the QENS near the elastic region permits an accurate measurement of $I(Q, E = 0)$ versus Q over the range 0.36–2.52 $\mathrm{\AA}^{-1}$ (except for removing data from a handful of detectors that are contaminated either by electronic noise or by incomplete subtraction of the Bragg reflections from the SWNTs); hence the characterization of the mean-square displacement of hydrogen atoms of nanotube-water. Furthermore, the monitoring of the quasielastic scattering component by the QENS allows a study of the diffusion/relaxation processes of hydrogen atoms.

When assessing the scattered intensity from hydrogen atoms, the background scattering from the sample holder and the nanotube host were removed by subtracting the corresponding empty-holder and dry-nanotube runs from the nanotube-water data. During each experiment, the sample was enclosed in an air-tight holder. The sample assembly was attached to a closed-cycle helium refrigerator for cooling and the temperature was controlled to within 1 K. Measurements of neutron standards (vanadium, D_2O, Cd absorber, etc) provided incident-spectrum normalization, detector calibration and correction for sample attenuation.

2.3. Molecular-dynamics simulations

MD simulations of water in SWNTs were performed on a rigid (10, 10) SWNT of 13.8 Å in diameter and 40 Å in length enclosing 126 water molecules. Periodic boundary conditions were applied to take care of surface effects. The water–carbon and water–water interactions were represented by a Lennard-Jones (LJ) and the TTM2-F polarizable flexible water model, respectively, both of which were validated separately by experiments [13–15]. The TTM2-F polarizable flexible water model, using smeared charges and dipoles to model short-range electrostatics, was able to accurately account for the high-level electronic structure data of water clusters and to reproduce the bulk behaviour of ice and ambient liquid water. For comparison MD simulations of ice-I*h* and liquid water were carried out using the TTM2-F model. An Ewald sum was used to incorporate the long-range Coulomb interactions. The hydrogen vibrational DOS and mean-square displacements were calculated following standard procedures.

Achieving ergodicity is one of the most challenging problems in computational statistical mechanics. Conventional single-trajectory molecular dynamics tends to get stuck in local regions of phase-space and cannot easily locate low-lying minima such as crystalline structures. To circumvent this problem we employed a 'parallel tempering' molecular dynamics (PTMD) algorithm [16] taking advantage of the parallel-computing capabilities of Argonne's Jazz

computer cluster. The PTMD algorithm calculates simultaneously multiple trajectories, each assigned to a different temperature; occasionally swapping temperatures between neighbouring trajectories is administered (in accordance with detailed balance under the Boltzmann distribution), effectively allowing the system to heat up temporarily to escape over intermediate local barriers and then to cool down for annealing in the vicinity of low-energy regions of the potential energy surface. This technique proved to be essential to assess structural variations and dynamic processes over a wide range of temperatures and pressures for comparison with experimental results.

3. Experimental results

We first present the neutron data in figures 2(a), 3(a), (b) and 4(a) and discuss the significance of the findings in the following three subsections. The results of the MD simulations are shown side by side with the data in figures 2(b), 3(c) and 4(b) to facilitate the comparison between calculation and experiment. However, the unique structure and dynamics of nanotube-water, which are brought out collectively by the experiments and simulations, are best described together. Hence they will be presented in the next section along with those investigations by other authors.

3.1. Encapsulation of water in SWNTs

Experimental verification of the presence of water inside SWNTs was achieved by wide- and small-angle neutron diffraction. In wide-angle diffraction, any revelation of diffraction peaks corresponding to the crystalline D_2O ice below 273 K would indicate the presence of bulk water outside of the SWNTs—a condition for rejecting a sample for further study. In small-angle neutron diffraction, the coherent scattering-length density was varied using different D_2O–H_2O mixtures in an SWNT sample, thereby providing the needed sensitivity to assess the structure and location of the water. When no bulk ice was detected by wide-angle diffraction, the location of the water was determined based on an analysis of the small-angle scattered intensity $I_{\mathrm{el}} \propto S(Q) \cdot f(Q)$ at 278 K, where $f(Q)$ is the form factor of an individual water-containing SWNT and $S(Q)$ the structure factor of the 2D hexagonal packing of the SWNTs in the bundles. The latter yields a first Bragg reflection, (01), at 0.41 $\mathrm{Å}^{-1}$ for our SWNT (14 Å diameter) which is clearly visible in the dry SWNT, figure 2(a). $f(Q)$, which is the Fourier transform of the scattering-length density of one SWNT and the associated water, exhibits a series of minima (zeros) in Q. The first zero for a dry SWNT occurs at Q of 0.385 $\mathrm{Å}^{-1}$. Assuming water is *inside* the nanotube, at a fixed ∼10 wt% of water in the SWNT, the first zeros occur at 0.385, 0.4, and 0.41 $\mathrm{Å}^{-1}$, for water compositions of 100% H_2O, 50% H_2O–50% D_2O, and 100% D_2O, respectively. Consequently, the expected intensity of the above samples will decrease gradually as the minimum of $f(Q)$ and the maximum of $S(Q)$ coincide. This was indeed observed, as shown in figure 2(a). On the other hand, if water resides outside the nanotubes, for example, in the pores in between the tubes, the minimum of $f(Q)$ would occur at 0.385, 0.38 and 0.37 $\mathrm{Å}^{-1}$ for the corresponding hydrated samples, which would preserve the maximum at 0.4 $\mathrm{Å}^{-1}$ contrary to the observation. Assured by this analysis, we established an optimal H_2O/SWNT mass ratio of 11.3% for our nanotube-water samples that contain only encapsulated water inside the nanotubes.

3.2. Inelastic spectra

The hydrogen vibrational DOS for nanotube-water was measured on the HRMECS and extracted from the difference between the inelastic neutron scattering (INS) intensities of

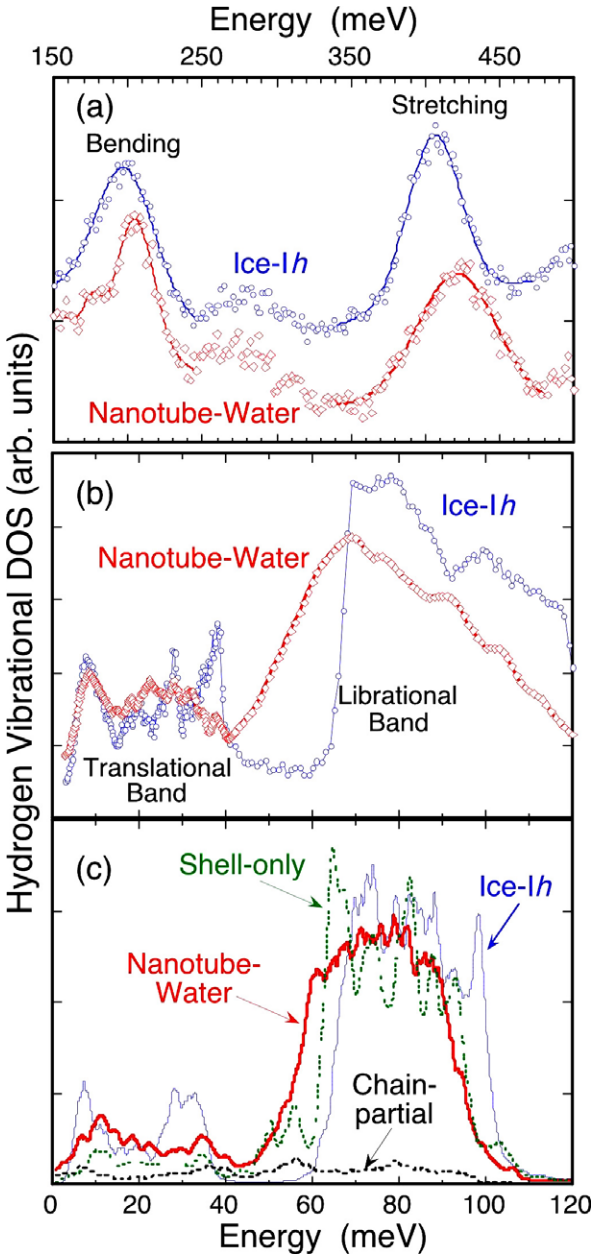

Figure 3. The observed neutron-weighted hydrogen vibrational DOS of nanotube-water and ice-Ih at 9 K: (a) the bending and stretching band and (b) the translational and librational band. (c) The corresponding simulated DOS for nanotube-water and ice-Ih. Chain-partial is the partial DOS from the chain contribution and shell-only is the DOS from a separated MD simulation for only a shell of water in SWNT.

11.3 wt%-H_2O SWNT and dry SWNT samples, at 9 K. These data were compared to the reference bulk ice-Ih DOS measured at the same temperature on the same spectrometer. Figure 3(a) shows the spectrum from using incident neutron energy of 600 meV, probing the intramolecular O–H stretch and H–O–H bending modes. These modes, located at respectively 406 and

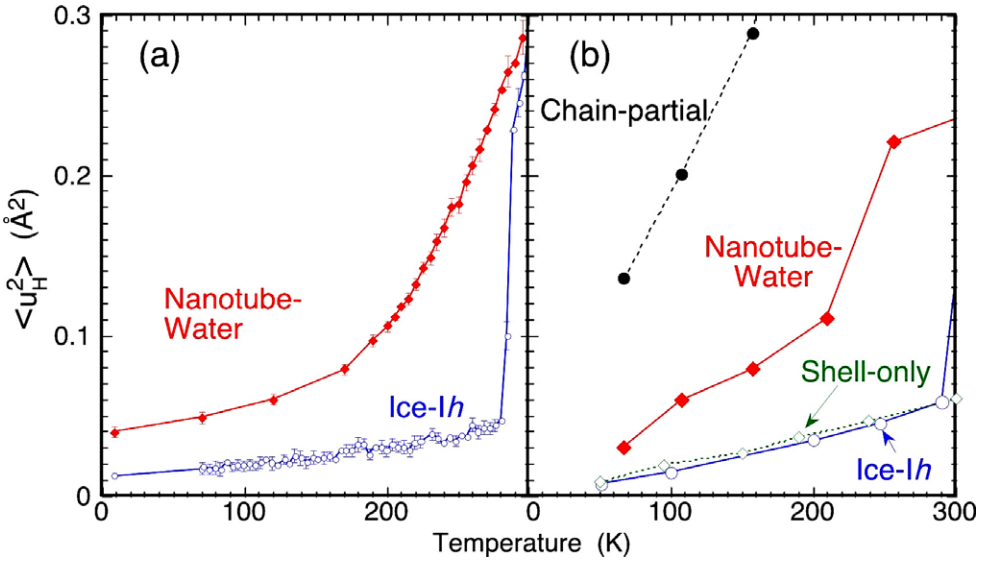

Figure 4. The observed (a) and simulated (b) hydrogen mean-square displacements $\langle u_H^2 \rangle$ for nanotube-water and ice-I*h*. The simulated $\langle u_H^2 \rangle$ for hydrogen atoms in the chain of nanotube-water and in the shell-only configuration are also given in (b).

199 meV in ice-I*h*, are noticeably shifted to higher energies in nanotube-water, i.e. 422 and 205 meV. These blue shifts imply a shorter intramolecular O–H bond length in nanotube-water compared to that in bulk ice-I*h*, and from the phenomenological model of Klug and Whalley [17] we estimate the O–O distance between nanotube-water molecules to be 2.916 Å, more than that (2.76 Å) for ice-I*h*. Such large variations imply a weakened hydrogen-bond network in nanotube-water, corresponding to a different structure as compared to bulk hexagonal ice-I*h*. In the extreme case of complete absence of hydrogen bonds in water vapour, the O–H stretch frequency increases to 469 meV. The weakened hydrogen-bonding of nanotube-water is consistent with the observed strongly damped intensities of these modes with increasing Q. As mentioned in section 2.2, this damping is controlled by the magnitude of the hydrogen mean-square displacement $\langle u_H^2 \rangle$ via the factor $\exp(-\langle u_H^2 \rangle Q^2)$, and indeed a weakened hydrogen-bonding is necessary for observing a large $\langle u_H^2 \rangle$ in nanotube-water (a more quantitative assessment of $\langle u_H^2 \rangle$ is discussed below). These results are corroborated by our observed intermolecular bands of nanotube-water at incident neutron energies of 140 and 50 meV. These data are shown in figure 3(b), where the ice-I*h* and nanotube-water spectra are compared. In this energy region, the well-defined band of translational modes below 40 meV and a librational band rising up sharply above 64 meV are characteristic of bulk ice-I*h*. In nanotube-water the DOS is shifted overall towards lower energies, with its librational band rising slowly at 40 meV (the midpoint of onset is at 55 meV), and its translational modes are softened to form a broadened band with much less weight at 35–40 meV. Hence these red shifts of the intermolecular modes support, as the blue shifts of the intramolecular modes do, the weakening of the hydrogen-bonded water network in nanotube-water. Therefore, relatively to its bulk ice-I*h* counterpart, the hydrogen vibrational DOS of water appears profoundly affected by the confinement in SWNTs.

3.3. Mean-square displacements of hydrogen

Hydrogen mean-square displacements $\langle u_H^2 \rangle$ were obtained by fitting the measured elastic intensity integrated over from -0.2 to 0.2 meV by the QENS to the expression of equation (1).

$\langle u_H^2 \rangle$ is a good measure of the hydrogen vibration amplitude provided that atomic migration from one molecule to another and molecular diffusion do not happen; otherwise, the hydrogen motion is better quantified by the analysis of the quasielastic scattered intensity which is monitored concurrently on the QENS. The $\langle u_H^2 \rangle$ for ice-I*h*, as shown in figure 4(a), increases slowly at a rate almost constant with temperature up to the melting temperature of 273 K, reflecting a temperature dependence for which hydrogen vibrations are approximated by harmonic oscillations. The abrupt jump of $\langle u_H^2 \rangle$ at 273 K arises from melting of ice-I*h*. The $\langle u_H^2 \rangle$ of nanotube-water (11 wt% H_2O in SWNT), as shown also in figure 4(a), differs drastically from that of ice-I*h*. The values are much higher, about four times as large at 8 K, increasing nearly linearly with rising temperature until about 200 K then escalating much faster at higher temperatures. The curve of $\langle u_H^2 \rangle$ is smooth but it displays a change of the slope around 210 ± 10 K. This, in conjunction with the appearance of a quasielastic scattering component above ∼210 K, suggests a sluggish change of the nature of hydrogen dynamics in nanotube-water from predominately local vibrations to diffusive motion.

4. Discussion

We first address the time-averaged (static) structure of nanotube-water. The neutron low-Q diffraction data show unequivocally that water can enter the open-ended SWNTs and nanotube-water samples can be prepared according to our method of preparation. Further insight into the structure of the nanotube-water was obtained from the MD simulations. Figure 2(b) shows the free energy across the nanotube walls for nanotube-water at 100 K. The hydrophobic interaction between the nanotube wall and water, represented by the LJ potential, facilitates an energy minimum at ∼3.2 Å from the wall. Water molecules after entering the nanotube will first condense and form a cylindrical shell—a tube-in-tube structure. Below ∼210 K, water molecules on the shell exhibit a fourfold coordinated 'square-ice' pattern. However, as the water density increases, the energy required for adding water molecules inside the square-ice shell reduces rapidly. Eventually, a local minimum of the free energy is realized at the centre of the nanotube (see figure 2(b)). The resulting time-averaged, final shell–chain configuration of nanotube-water is shown in figure 2(c) [18]. Due to the one-dimensional character of the chain, the mean coordination number for the chain water molecules is only 1.86, which is much less than the 4- and 3.8-coordination for bulk ice and liquid water, respectively.

In their simulations Koga *et al* found the water shell inside the nanotube as a stable structure but did not identify the central water chain [19]. It is possible that the small energy gain associated with the addition of the central water chain had not been detected in their initial study. More recently, Tanaka and Koga [20] showed computer simulation results supporting the occupancy of hydrophobic guest molecules such as argon and methane in the centre of the ice shell.

It is important to recognize the extraordinary large $\langle u_H^2 \rangle$ in nanotube-water—about four times of that in ice-I*h* even at 8 K—when considering the static structure of nanotube-water. Hydrogen atoms in nanotube-water undergo anomalously large-amplitude vibrations, momentarily breaking some hydrogen bonds or forming new ones, especially at increasing temperatures. Therefore, the picture in figure 2(c) should be regarded as an idealized configuration of the shell–chain structure at low temperatures. Figure 5 shows a snapshot of nanotube-water at 100 K, emphasizing the relatively different strength of hydrogen bonds, i.e., strong network-forming hydrogen bonds among the shell molecules versus the weak, fluctuating ones among the chain molecules or connecting the shell and chain molecules. As the temperature rises over about 210 K, MD results show a 'melt-down' of the shell–chain structure resulting in diffusion of water molecules as in liquid water. This is illustrated by the

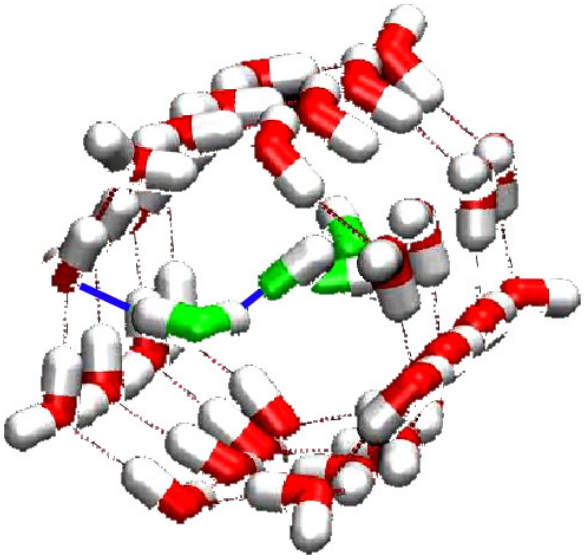

Figure 5. A snapshot from an MD simulation of nanotube-water at 100 K illustrating the relative strength of hydrogen bonds—the strong ones (thin lines) in the shell and weak ones (thick lines) either connecting molecules in the chain or cross-linking molecules from the shell and the chain.

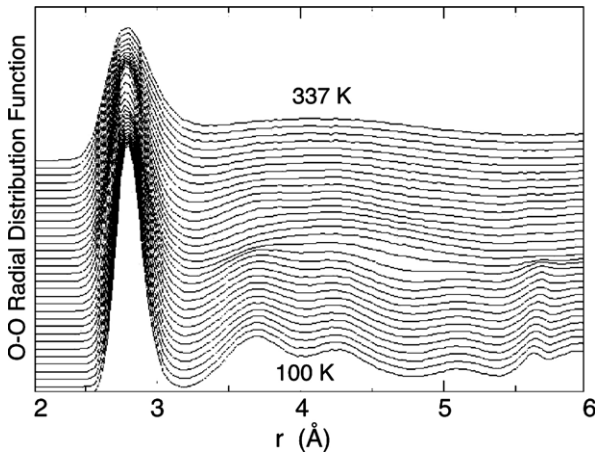

Figure 6. Temperature dependence of the O–O RDF function, calculated from the PTMD simulations of nanotube-water from 100 to 337 K with a uniform temperature step. Each temperature trace is displaced upwards for the sake of clarity. Intermediate-range order, manifested in O–O correlation beyond the nearest neighbours, gradually disappears above ∼210 K, indicating the transformation of the shell–chain structure to supercooled liquid water.

calculated temperature dependence of the O–O radial distribution function (RDF) by PTMD simulations in figure 6.

The large extent of local disorder caused by the large-amplitude vibrations, especially the enhanced fluctuations of the chain molecules, and the small number of molecules in the chain (12.5% of the total number of molecules), underscore the difficulty in a direct determination of the static structure using diffraction methods. All the salient features in the O–O RDF at low temperatures, as shown in figure 6, arise from the shell because O–O correlation in the shell

dominates the short-to-intermediate-range order. Therefore, it is not surprising that the x-ray diffraction experiments on nanotube-water carried out by Maniwa *et al* showed strong evidence of the shell but not the central chain based on their interpretation of the x-ray data [21, 22]. However, that is not to say that the chain component is not important in nanotube-water. In fact, on the contrary, it is the chain component that provides a satisfactory account of the anomalous dynamic behaviour of nanotube-water observed by inelastic scattering.

We devised MD simulations to assess the contributing factors to the anomaly in the vibrational DOS of nanotube-water. In addition to simulation of the nanotube-water and the ice-I*h* reference, we calculated the partial DOS from the chain in nanotube-water and simulated a shell-only configuration in SWNT. The shell-only situation may not bear any physical reality but it allows a qualitative evaluation of the relative hydrogen-bond energetics of the shell and shell–chain configurations. Figures 3(b) and (c) show a comparison of the intermolecular modes from MD simulations and neutron experiments. The shoulder above 100 meV in the experimental data contains a substantial contribution from combined excitations of the translational band and the librational band. Bearing in mind that the MD spectra do not include combination modes, the agreement between the observed and MD spectra is good for both nanotube-water and ice-I*h*. Specifically, the simulated DOS of nanotube-water clearly accounts for the smearing of the translational band and the filling of intensity in the 40–70 meV region of the librational band relative to those bands of ice-I*h*.

For the simulated spectra in figure 3(c), the shell-only spectrum agrees better with nanotube-water than with ice-I*h*. But the sum of the shell-only spectrum and the chain-partial spectrum does not account for the softening of the librational band around 60 meV. The best agreement between experiment and simulation is achieved only by the shell–chain model that inherently includes the shell–chain interaction via exchange of hydrogen bonds.

As the temperature rises, dynamic fluctuations of hydrogen bonds between the square-ice shell network and the chain increase. Above ∼210 K the shell–chain structure vanishes and nanotube-water behaves, to a certain extent, like supercooled liquid water that supports long-range molecular diffusion. In the liquid-like state, enhanced fluctuations lead to a large distribution of distorted hydrogen-bond configurations, hence diminishing the intermediate-range order, as can be seen in the calculated O–O RDF (see figure 6).

The MD simulations of the hydrogen-bond dynamics in terms of the mean-square displacements of hydrogen atoms, $\langle u_{\mathrm{H}}^2 \rangle$, is equally revealing. Figure 4(b) shows the simulated $\langle u_{\mathrm{H}}^2 \rangle$ for nanotube-water, ice-I*h*, as well as the shell-only and chain-partial configurations. The classical treatment in the simulations demands zero $\langle u_{\mathrm{H}}^2 \rangle$ at 0 K. Hence, the MD results, for the lack of zero-point energy, cannot be compared quantitatively with experimental data at very low temperatures. The $\langle u_{\mathrm{H}}^2 \rangle$ of ice-I*h*, being the smallest in magnitude, reproduces the linear temperature dependence and the abrupt rise at melting as observed experimentally. The $\langle u_{\mathrm{H}}^2 \rangle$ of nanotube-water evaluated at 50, 100, 150, 250 and 300 K, on the other hand, shows overall higher values, a break of the slope at about 200 K, and no abrupt jump near the ice melting point, which agree qualitatively with all the key features from experiment. The chain-partial $\langle u_{\mathrm{H}}^2 \rangle$ rises steeply and takes off to a much larger value at the onset of diffusive motion at ∼160 K. Simulations also show that the shell-only $\langle u_{\mathrm{H}}^2 \rangle$ behaves like ice-I*h* up to the melting point. Because shell–chain interactions are missing in the shell-only configuration, the simulation may overemphasize the stiffness of the shell. Nevertheless, the simulations show clearly the differing dynamics—the stiff versus soft hydrogen bonds in the shell and chain at low temperatures, the enhanced shell–chain interactions with increasing temperature, and their melting into liquid-like water above ∼210 K.

To summarize, we reiterate the following observations. First, INS provides one of the most sensitive means for assessing the different structures of water [23, 24]. Second, the validation

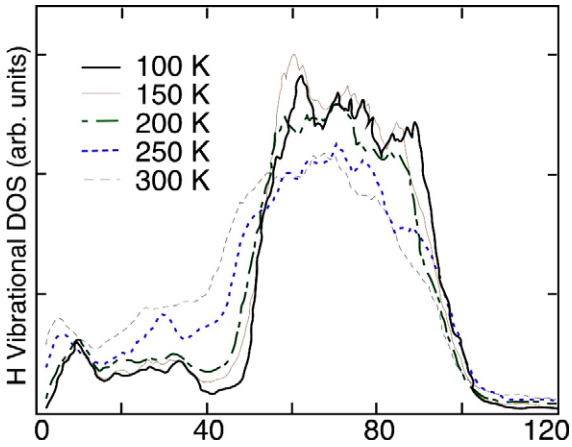

Figure 7. MD simulated H vibrational DOS of nanotube-water at selected temperatures.

of the TTM2-F potential for water is demonstrated by the excellent agreement with the binding energies of small water clusters and also by good reproducibility of the bulk structure and the vibrational DOS of ice and ambient liquid water [14, 15]. Finally, the good agreement between the observed and calculated INS spectra and $\langle u_{\mathrm{H}}^2 \rangle$ for nanotube-water, as shown in figures 3 and 4, achievable only by the shell–chain model, lends unequivocal credence to our assertion of the shell–chain structure of nanotube-water at temperatures below ∼210 K.

The nature of the structural change of water in SWNTs (14 Å in diameter) was investigated by proton NMR measurements carried out by Ghosh *et al* over the temperature range 200–300 K [25]. Two onset temperatures of 242 and 212 K were identified. However, the authors' interpretation of depletion of water molecules from the central chain to the shell below 242 K and complete freezing of the hollow shell at 212 K cannot be reconciled with our neutron data and MD simulation results. The hydrogen vibrational DOS and mean-square displacements are very sensitive to differentiate the hydrogen-bond dynamics between nanotube-water and bulk ice/water. The PTMD method permits the calculations of the spectral changes in the DOS as a function of temperature. Figure 7 shows a strong increase in intensity of the low-energy modes and large shift of the librational band towards lower energies above 200 K, which underlines the importance of the shell–chain dynamics towards the melting transition at ∼210 K. Over the entire temperature range the nanotube-water spectra clearly differ from those of bulk ice.

5. Conclusions

A combined neutron-scattering and molecular-dynamics-simulation study was carried out to investigate the structure and dynamics of water confined in open-ended SWNTs (nanotube-water). As shown in numerous previous experiments, the hydrogen vibrational DOS obtained from INS is very sensitive to subtle structural differences in different phases of water that lack a long-range order structure. Using the parallel tempering MD technique, we investigated the stable configurations of nanotube-water at different temperatures and compared the simulation results quantitatively with the neutron data, reaching a scenario consistent with all the experimental observations as follows. A shell + chain configuration of nanotube-water was identified at temperatures below ∼210 K. The shell consists of a square-ice sheet rolled into a hollow cylinder parallel to the SWNT long axis in a tube-in-tube configuration. A gap of ∼3 Å is maintained between the nanotube wall and the

shell as a direct consequence of the hydrophobic interaction between the water molecules and carbon atoms. In the centre of the shell a single file of water molecules is situated with an average coordination number of 1.86, hence forming a central chain. Large fluctuations via hydrogen-bond breaking/formation, including those associated with molecules between the shell and the chain, prevail and the resulting overall hydrogen-bond network of nanotube-water is weakened significantly even at very low temperatures. Hydrogen bonds associated with the chain are especially pliable. The fluctuations increase drastically with temperature and eventually at ∼210 K the shell–chain structure transforms to liquid-like supercooled water. Although the present classical MD simulation cannot address any additional quantum effects in nanotube-water, the experimental observation of a $\langle u_{\mathrm{H}}^2 \rangle$ four times larger than that of ice-I*h* at 10 K strongly suggests that, in an environment of significantly weakened hydrogen bonds, nanotube-water must display a highly delocalized ground-state wavefunction and a reduced kinetic energy of the protons. This interesting aspect is currently the subject of an investigation by neutron deep-inelastic scattering and quantum MD simulations.

What are the similarities and differences between water confined in SWNTs and MCM-41-S, both featuring 14 Å-diameter pores? An obvious difference is the nonwetting behaviour of water on the nanotube carbon surfaces. Conceptually, supercooled nanotube-water (above 210 K) without any direct bonding with the nanotube substrate may behave more closely to bulk water and therefore the system would facilitate systematic studies of the anomalous properties of water over the no man's land. Thus far neutron-scattering experiments have not yet been carried out to the extent affording full comparison with the water in MCM-41-S. However, initial results are encouraging. Our preliminary inelastic-scattering study shows a spectral change of the hydrogen vibrational DOS in nanotube-water qualitatively similar to that of water in MCM-41-S [26] as the systems enter the supercooled state from low temperatures. We also performed quasielastic scattering measurements of the relaxation processes in supercooled water using neutron backscattering spectrometry [27]. The initial results show a crossover at 218 K from a Vogel–Fulcher–Tamman (VFT) law to an Arrhenius behaviour typical of a fragile-to-strong liquid transition in confined water, compared to 224 K for water in MCM-41-S. The activation energy of 5.4 kJ mol^{-1}, obtained from the Arrhenius behaviour at low temperature, is 3.8 times smaller than that for water in MCM-41-S. Clearly, more neutron and MD investigations over extended temperature and pressure regimes are needed to clarify the nature of the transition in nanotube-water.

Finally, we point out that both the structure and dynamics of water in carbon nanotubes are critically influenced by the size of the confining space. So far most experiments have been performed on 14 Å diameter nanotubes. Our MD simulations of water in (9, 9) SWNTs of 12.5 Å diameter predict only the shell structure of water inside the nanotubes. Furthermore, water confined in double-wall carbon nanotubes of 16 Å diameter obeys the VFT law down to at least 195 K. Therefore, water confined in different carbon nanotubes appears to conform to different structures and to exhibit distinct relaxation processes and vibrational motion. We anticipate a rich future development in this field by experiments and computer simulations.

Acknowledgments

We thank Alexander P Moravsky, Raouf O Loutfy of MER Corporation for supplying the high-purity carbon nanotube samples. Helpful discussions with Jean-Marc Zannoti, (LLB) Pappannan Thiyagarajan (ANL), Eugene Mamontov (NIST) and George Reiter (University of Houston) are gratefully acknowledged. The work performed at the Intense Pulsed Neutron Source was supported by the Office of Basic Energy Sciences, Division of Materials Sciences,

US Department of Energy, under Contract No. W-31-109-ENG-38. The work of CJB was performed under the auspices of the DOE Grant DE-FG02-03ER46078.

References

[1] Debenedetti P G and Stillinger F H 2001 *Nature* **410** 259
[2] Finney J L 2004 *Phil. Trans. R. Soc.* B **399** 1145
[3] Liu L, Chen S-H, Faraone A, Yen C-W and Mou C-Y 2005 *Phys. Rev. Lett.* **95** 117802
[4] Xu L, Kumar P, Buldyrev S V, Chen S-H, Poole P H, Sciortino F and Stanley H E 2005 *Proc. Natl Acad. Sci. USA* **102** 16558
[5] Gallo P, Rovere M and Spohr E 2000 *J. Chem. Phys.* **113** 11324
[6] Scatena L F, Brown M G and Richmond G L 2001 *Science* **292** 908
[7] Bellessent-Funel M-C, Sridi-Dorbez R and Bosio L 1996 *J. Chem. Phys.* **104** 10023
[8] Kong Y and Ma J 2001 *Proc. Natl Acad. Sci. USA* **98** 14345
[9] Pomes R and Roux B 2002 *Biophys. J.* **82** 2304
[10] Lanyi J K 2000 *J. Chem. Phys.* **104** 11441
[11] Chiang I W, Brinson B E, Huang A Y, Willis P A, Bronikowski M J, Margrave J L, Smalley R E and Hauge R H 2001 *J. Chem. Phys.* **105** 8297
[12] Tomkinson J 1994 *The INS Spectroscopy of Hydrogen Bonds* ed A Furrer (Singapore: World Scientific) p 168
[13] Walther J H, Jaffe R, Halicioglu T and Koumoutsakos P 2001 *J. Phys. Chem.* B **105** 9980
[14] Burnham C J and Xantheas S S 2002 *J. Chem. Phys.* **116** 5115
[15] Burnham C J and Xantheas S S 2002 *J. Chem. Phys.* **116** 1500
[16] Sugita Y and Okamoto Y 2000 *Chem. Phys. Lett.* **329** 261
[17] Klug D D and Whalley E 1984 *J. Chem. Phys.* **81** 1220
[18] Kolesnikov A, Zanotti J-M, Loong C-K, Thiyagarajan P, Moravsky A P, Loutfy R O and Burnham C J 2004 *Phys. Rev. Lett.* **93** 35503
[19] Koga K, Gao G T, Tanaka H and Zeng X C 2001 *Nature* **412** 802
[20] Tanaka H and Koga K 2005 *J. Chem. Phys.* **123** 094706
[21] Maniwa Y, Kataura H, Abe M, Suzuki S, Achiba Y, Kira H and Matsuda K 2002 *J. Phys. Soc. Japan* **71** 2863
[22] Maniwa Y, Kataura H, Abe M, Udaka A, Suzuki S, Achiba Y, Kira H, Matsuda K, Kadowaki H and Okabe Y 2005 *Chem. Phys. Lett.* **401** 534
[23] Li J C 1996 *J. Chem. Phys.* **105** 6733
[24] Tse J S, Klug D D, Tulk C A, Swainson I, Svensson E C, Loong C-K, Shpakov V, Belosludov V R and Kawazoe Y 1999 *Nature* **400** 647
[25] Ghosh S, Ramanathan K V and Sood A K 2004 *Europhys. Lett.* **65** 678
[26] Liu L *et al* 2006 *J. Phys.: Condens. Matter* **18** S2261
[27] Mamontov E, Burnham C J, Chen S-H, Moravsky A P, Loong C-K, de Souza N R and Kolesnikov A I 2006 *J. Chem. Phys.* **124** 194703